IEEE Access
Multidisciplinary | Rapid Review | Open Access Journal

Received January 3, 2019, accepted February 2, 2019, date of publication February 7, 2019, date of current version February 27, 2019.

Digital Object Identifier 10.1109/ACCESS.2019.2898111

A Phase Congruency and Local Laplacian Energy Based Multi-Modality Medical Image Fusion Method in NSCT Domain

ZHIQIN ZHU[1], MINGYAO ZHENG[1,2], GUANQIU QI[3], DI WANG[4], and YAN XIANG[1,2]

[1]Key Laboratory of Industrial Internet of Things and Networked Control, Ministry of Education, College of Automation, Chongqing University of Posts and Telecommunications, Chongqing 400065, China
[2]Faculty of Information Engineering and Automation, Kunming University of Science and Technology, Kunming 650504, China
[3]Department of Mathematics and Computer and Information Science, Mansfield University of Pennsylvania, Mansfield, PA 16933, USA
[4]School of Communication Engineering, Chongqing University, Chongqing 400044, China

Corresponding author: Yan Xiang (reilove2@outlook.com)

This work was supported in part by the National Natural Science Foundation of China under Grant 61803061 and Grant 61703347, in part by the Science and Technology Research Program of Chongqing Municipal Education Commission under Grant KJQN201800603, in part by the Major Science and Technology Project of Yunnan Province under Grant 2018ZF017, in part by the Chongqing Natural Science Foundation under Grant cstc2018jcyjAX0167, in part by the Common Key Technology Innovation Special of Key Industries of Chongqing Science and Technology Commission under Grant cstc2017zdcy-zdyfX0067 and Grant cstc2017zdcy-zdyfX0055, and in part by the Artificial Intelligence Technology Innovation Significant Theme Special Project of Chongqing Science and Technology Commission under Grant cstc2017rgzn-zdyfX0014 and Grant cstc2017rgzn-zdyfX0035.

ABSTRACT Multi-modality image fusion provides more comprehensive and sophisticated information in modern medical diagnosis, remote sensing, video surveillance, and so on. This paper presents a novel multi-modality medical image fusion method based on phase congruency and local Laplacian energy. In the proposed method, the non-subsampled contourlet transform is performed on medical image pairs to decompose the source images into high-pass and low-pass subbands. The high-pass subbands are integrated by a phase congruency-based fusion rule that can enhance the detailed features of the fused image for medical diagnosis. A local Laplacian energy-based fusion rule is proposed for low-pass subbands. The local Laplacian energy consists of weighted local energy and the weighted sum of Laplacian coefficients that describe the structured information and the detailed features of source image pairs, respectively. Thus, the proposed fusion rule can simultaneously integrate two key components for the fusion of low-pass subbands. The fused high-pass and low-pass subbands are inversely transformed to obtain the fused image. In the comparative experiments, three categories of multi-modality medical image pairs are used to verify the effectiveness of the proposed method. The experiment results show that the proposed method achieves competitive performance in both the image quantity and computational costs.

INDEX TERMS Medical image fusion, multi-modality sensor fusion, NSCT, phase congruency, Laplacian energy.

I. INTRODUCTION

As a powerful and fundamental tool, medical imaging plays an irreplaceable role in modern medical diagnosis and treatment. A number of medical imaging modalities, that include positron emission tomography (PET), computed tomography (CT), and magnetic resonance imaging (MRI), are implemented to address different lesions of cells or organs. Since each medical imaging modality has it own purposes, strengths, and limitations, one modality cannot usually provide sufficient information for a whole medical diagnosis.

Medical image fusion encompasses a broad range of general image fusion techniques to integrate complementary information from different modalities of medical images. It offers a great diversity of image features for medical analysis, and often leads to the robust medical diagnosis. The additional information acquired from the integrated images can be well utilized to precisely discover the position of lesion.

The associate editor coordinating the review of this manuscript and approving it for publication was Yuming Fang.

Due to the high requirements of multi-modality medical image fusion, a number of fusion techniques has been developed in the last few years. Generally, image fusion techniques can be categorized into two classes, such as spatial and transform domain methods [34], [41].

According to the characteristics of spatial information, spatial domain methods select image pixels or patches from each source image to construct a fused image. For spatial domain methods, the detailed information of source images can be perfectly preserved. All the information preserved in the fused image is same as the original one in source images. Since spatial domain methods can completely preserve the spatial information of source images, they have state-of-the-art performance in multi-focus [15], [17], [48] and multi-exposure [27], [28] image fusion. However, the shortcoming of spatial domain methods is also obvious. Spatial domain fusion methods can hardly integrate the information from the same position in each source image, other than image pixel weighted average methods [14], [16]. But the image pixel weighted average methods often cause the contrast and sharpness decreasing of detailed information in fused image that is not acceptable in medical image fusion.

In multi-modality medical image fusion, transform domain based methods are commonly used [47], [52]. Unlike spatial domain methods, transform domain methods transform source images into specific coefficients first. Then they fuse the coefficients, and inversely transform all the fused coefficients into a fused image. Sparse representation and multi-scale transform (MST) based methods have become the most popular image fusion solutions in recent years. MST-based algorithm is a frequency domain method in image processing. This algorithm decomposes source images into high and low frequency by transform (such as CVT, NSCT and NSST), and then designs different fusion rules for high and low frequency to obtain the fused image. The sparse representation based algorithm is an image time domain processing method that obtains the sparse coefficients of source images through dictionary learning. The sparse representation and MST transform decompose source images in time domain and frequency domain respectively. Both of them are mainstream image fusion methods in the transform domain.

Sparse representation based methods are mainstreams in transform domain based multi-modality image fusion methods. Liu *et al.* [25] proposed an adaptive sparse representation based method for both medical and other kinds of multi-modality image fusion. It classified the trained dictionary bases into several categories according to the gradient information. Based on the joint patch clustering, Kim *et al.* [13] designed an efficient dictionary learning method for sparse representation based image fusion. It achieved great performance as the trained dictionary can perfectly describe the detailed information of source images. Furthermore, the dictionary learning method proposed by Kim can obtain a compact trained dictionary that can effectively reduce the computation costs. Li *et al.* [14] proposed a low-rank and sparse dictionary learning method for noisy medical image fusion. This method incorporated low rank and sparse regularization into dictionary learning model to enhance the detailed information. In sparse representation based image fusion, source images are sparsely coded as sparse coefficients by using simple $Max - l_1$ fusion rule, that makes the fused image keep excellent detailed information. However, the computation costs of sparse representation based methods are usually 2 to 3 times higher than other transform domain methods.

MST is the most popular algorithm in transform domain based image fusion. In multi-modality medical image fusion, MST-based methods, such as wavelet transform (DWT) [29], curvelet transform (CVT) [1], shearlet transform (ST) [22], non-subsampled contourlet transform (NSCT) [20], [24], and nonsubsampled shearlet transform domain (NSST) [35], [45] are commonly used. NSCT and NSST based multi-modality medical image fusion methods have obtained state-of-the-art performance in recent years. Liu *et al.* [24]proposed a general framework for multi-modality medical, infrared-visible, and multi-focus image fusion. In this framework, NSCT-based method obtained the best performance in multi-modality medical image fusion. Du *et al.* [9] proposed a method of fuse anatomical images and functional images. The method selected local Laplacian filtering as a multi-scale image decomposition tool for saving structural information and enhancing detailed information. Simultaneously, the merged approximate image and the residual image were respectively generated using the local energy maximum scheme and the interest scheme based information. Finally, a fused image was obtained using a reconstruction process similar to the traditional Laplacian pyramid transform. A multi-modal image fusion framework in NSCT domain was proposed [39]. In this framework, sparse representation was applied to merge the low-frequency coefficients. However, the high-pass subband fusion rule was based on the larger local energy or variance, which cannot effectively solve the smoothing issue of image details caused by SR. The multi-modal image fusion issue was solved by the variable weight fusion rule based on non-subsampled contour transform (NSCT) [19]. The algorithm combined the intensity of components of source images into a multi-scale space and obtained the fused image under the generalized intensity-hue-saturation (GIHS) framework. Source medical images were first decomposed into low- and high-frequency components in the NSCT domain [3]. The low-frequency components were then fused using an activity metric based on normalized Shannon entropy, while the high-frequency components were fused using directional contrast. This method preserved more spatial features and functional information, as well as converted them into the fused image. In the NSCT-based medical image fusion method proposed by Ganasala and Kumar [10], the fusion rule of low-frequency subband coefficients was designed by using the maximum entropy of the square of local window coefficients. The maximum weighted and modified Laplacian was used to measure the activity level of high-frequency subband coefficients. Li *et al.* [20] proposed an image fusion framework based

on NSCT and sparse representation to enhance and preserve more details. This fusion framework fused lowpass components by using sparse representation. The rule based on Sum Modified-Laplacian was applied to the fusion of highpass components fusion. A medial image fusion method based on NSCT was proposed in [2] to enhance details and preserve more energy. In this method, the phase congruency was used to measure the activity level of low-frequency coefficients, while the directive contourlet contrast feature as the fusion rule was applied to the high-frequency coefficients. Based on NSCT and PCNN, Xia *et al.* [42] proposed a multi-model medical image fusion algorithm combined with SR and pulse coupling neural network(PCNN). Gong *et al.* [11] proposed an image fusion method to preserve more image structure information. NSST-based method proposed by Yin *et al.* [45] also performed well in multi-modality medical image fusion. Yin's method used NSST to filter source images into high- and low-frequency coefficients, and also kept the detailed information in the fusion of coefficients. In addition, it also enhanced the details of fused image. Comparing with sparse-representation based methods, MST-based methods run much faster. However, for MST-based methods, simple fusion rules cannot always successfully identify the detailed and structured information from coefficients, and may cause the degradation of image quality. So it is important to design an effective fusion rule for MST-based methods.

In order to better extract the details of medical images and save more image energy, this paper proposes a novel MST-based method. This novel fusion method enhances the computational efficiency and fusion performance, as well as improves the visual perception of images. The proposed method is designed in NSCT domain that is one of most effective MST algorithms for medical image fusion [24]. NSCT algorithm can transform source images into highpass and lowpass subddands that mainly consist of the detailed and structured information respectively. As only the detailed information remains in highpass subbands, the enhancement of detailed features is the key work for highpass subbands. In most cases, due to the limits of computation costs, not all the detailed information can be filtered into the highpass subbands. Thus, the lowpass subbands fusion needs to process both detailed and structured information. So a phase-congruency based fusion rule and a local Laplacian energy based fusion rule are proposed for the fusion of highpass and lowpass subbands respectively. These two fusion rules cannot only enhance the detailed features, but also preserve the structured information of source multi-modality images.

The main contributions of this paper can be concluded in following three aspects:

1) It proposes an effective image fusion rule for the high-frequency components in multi-modality medical image fusion. The fusion rule combines three low-level features such as local phase consistency, local abrupt metric, and local energy information, to enhance the detailed features of high frequency components. More high-frequency contrast and brightness features from source images can be preserved in the fused image.
2) It also proposes a low-frequency components image fusion rule that takes both the extraction of detailed features and the preservation of structured information into consideration. The proposed local Laplacian energy based fusion rule uses weighted local energy and weighted sum of Laplacian coefficients to measure the structured and detailed information of lowpass subbands respectively. The proposed fusion rule can extract more detailed and structured information of source images, and better preserve the low-frequency energy. Thereby it can improve the visual perception ability of fused image.
3) It proposes an effective MST-based multi-modality image fusion framework with low computation costs. The proposed fusion framework in NSCT domain is effective for both highpass and lowpass subbands, as appropriate fusion rules are proposed for the extraction of detailed features and the preservation of structured information respectively. Additionally, as all the proposed fusion rules and NSCT transform run with low computation costs, the proposed method not only obtains high-quality fused results, but also achieves low computation costs.

The rest sections of this paper are structured as follows: Section II demonstrates the related work of NSCT; Section III proposes the framework and explains the proposed method in detail; Section IV simulates comparative experiments and analyzes corresponding results; Section V concludes this paper.

II. RELATED WORK

A. NONSUBSAMPLED CONTOURLET TRANSFORM

Based on contourlet transform, nonsubsampled contourlet transform (NSCT) can overcome the frequency aliasing phenomenon caused by up- and down-sampling on contourlet transform [5], [18]. NSCT is a discrete image calculation framework that achieves shift-invariant, multi-scale, and multi-directionality by using non-subsampled pyramid filter banks (NSPFBs) and non-subsampled directional filter banks (NSDFBs) [18], [30], [51]. NSCT framework is shown in Fig. 1.

1) NON-SUBSAMPLED PYRAMID FILTER BANK

NSPFB used in NSCT is a two-channel nonsubsampled filter bank with no up- and down- sampling operation, which ensures NSCT has multi-scale and shift-invariant characteristics. The source images are decomposed by NSPFB to obtain low- and high- pass images on each decomposition level. Next, NSPFB iterative decomposition is performed on low-frequency image to achieve multi-scale decomposition. After NSPFB decomposition, $k+1$ sub-images, that have the same size as source images, are obtained. There are k high-frequency images and 1 low-frequency image. k is the number of NSPFB decomposition levels. Fig. 2 shows a schematic

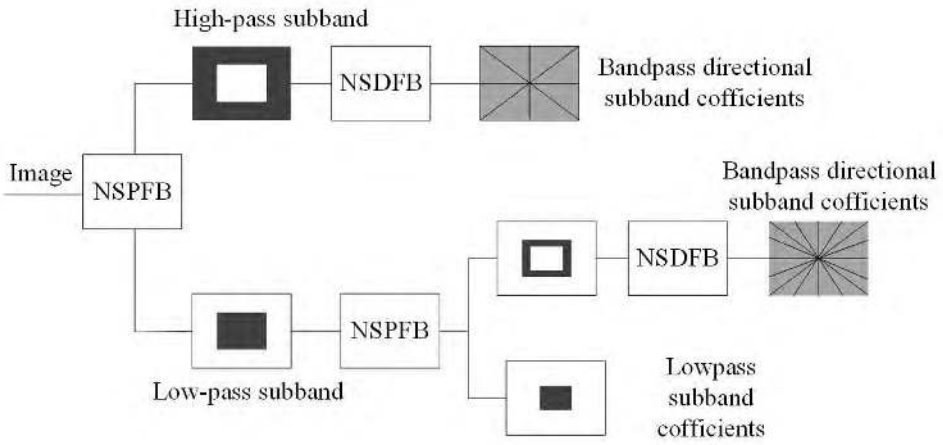

FIGURE 1. Nonsubsampled contourlet transform.

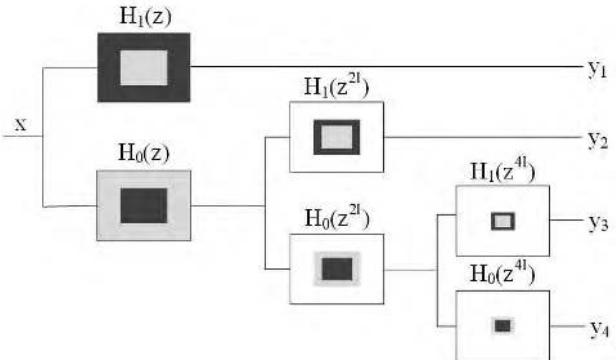

FIGURE 2. Non-subsampled pyramid filter bank.

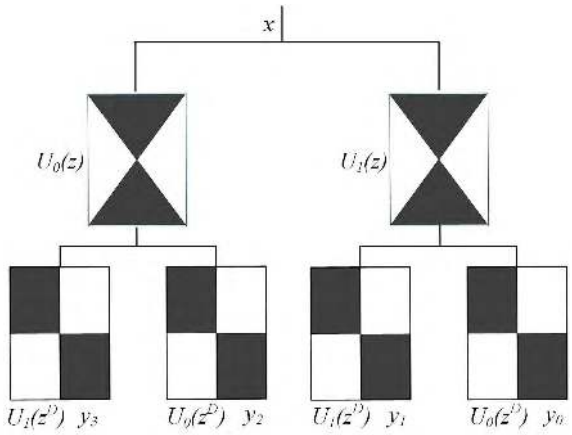

FIGURE 3. Non-subsampled directional filter bank.

diagram of NSPFB with three decomposition levels. The ideal frequency support area for the kth stage lowpass filter is:

$$\left[-\left(\pi/2^k\right)\ \left(\pi/2^k\right)\right]^2.$$

Eq. 1 gives the equivalent filter for K-level cascaded NSPDF.

$$H_n^{eq}(z) = \begin{cases} H_1(z^{2^{n-1}I})\Pi_{k=0}^{n-2}H_0(z^{2^kI}), & 1 \le n \le K \\ \Pi_{k-0}^{n-2}H_0(z^{2^kI}), & n = K+1 \end{cases} \quad (1)$$

where $H_0(z)$ and $H_1(z)$ denote the lowpass and corresponding highpass filter respectively.

2) NON-SUBSAMPLED DIRECTIONAL FILTER BANK

NSDFB is a two-channel tree-structured filter bank that is built by eliminating the downsampling and upsampling of directional filter bank. NSDFB performs l-level directional decomposition on the high-frequency image from NSPFB to obtain 2^l directional sub-images as same size as source images. This allows NSCT to obtain multi-directional characteristics and more accurate directional information. Fig. 3 shows the four-channel NSDFB. When the output of filter $U_j(z^D)(j = 0, 1)$ is combined with the output of first-stage fan filter $U_i(z)(j = 0, 1)$, four directional frequency decomposition can be obtained. The equivalent filter for each direction is given by Eq. 2. The synthesis filter bank is obtained similarly. All filter banks in NSDFB tree structure are obtained from a single nonsubsampled filter bank fan filters. In order to achieve multi-directional decomposition, NSDFB iterations can be applied to the highpass image obtained by NSPFB.

$$U_k(z) = U_i(z)U_j(z^D) \quad (2)$$

As shown in Fig. 1, NSCT is obtained by combining NSPFB and NSDFB. NSCT has multi-scale, multi-directional, and shift-invariant characteristics. The pseudo-Gibbs phenomenon can be avoided by introducing NSCT as an MST into image fusion. The subband maps decomposed by NSCT are as same size as source medical images, which is conducive to the design of high- and low-frequency fusion rules [6], [49].

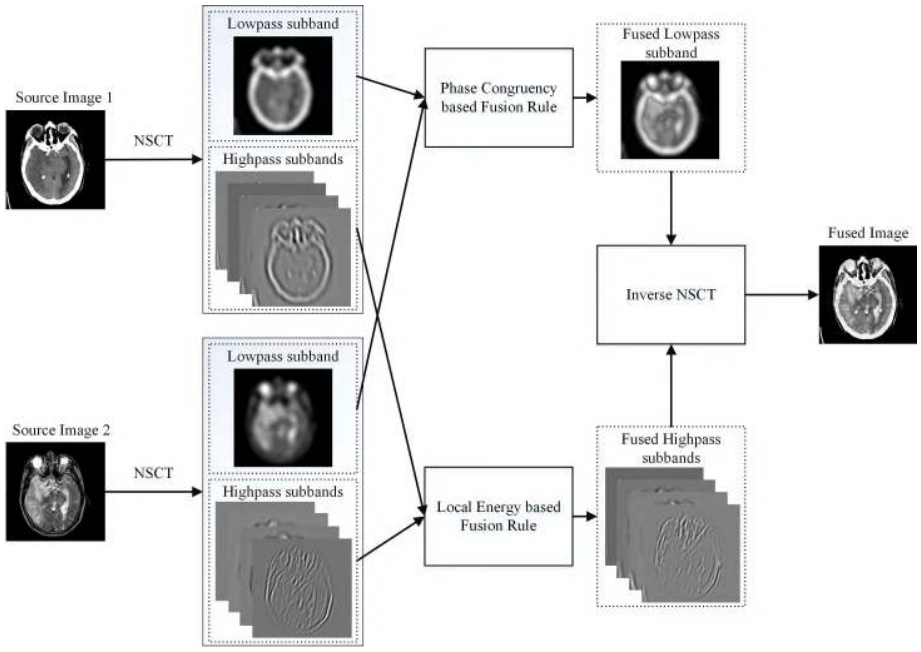

FIGURE 4. The proposed framework.

III. PROPOSED FRAMEWORK

In this paper, a novel MST-based multi-modality image fusion framework is proposed. The proposed method mainly consists of three steps that are NSCT decomposition, high- and low-pass subbands fusion, and inverse transformation as shown in Fig. 4. The first step of proposed method is image decomposition. The proposed method uses NSCT to decompose source images into high- and low-pass subbands that mainly describe the detailed and structured information respectively. In the second step, a phase congruency (*PC*) and local Laplacian energy based fusion rule are applied to the fusion of high- and low-pass subbands. The final step is to combine and inversely transform the fused high- and low-pass subbands. The details of proposed method are presented as follows.

A. FUSION RULE OF HIGHPASS SUBBAND

When the multi-modality medical image pairs are decomposed by NSCT, a proper fusion rule is needed to obtain an integrated image with better performance. The highpass subbands of NSCT filtered images mainly describe the detailed information that corresponds to the texture and edge information of source images. In medical imaging, organ and cell lesions are often identified by detailed information. Thus, the key of highpass subband fusion is to enhance the detailed features of each source image.

In this paper, to make the highpass subband image more informative, PC is implemented to enhance image features. *PC* is a dimensionless measurement that can measure the significance of image features. In highpass subbands, PC value corresponds to the sharpness of image object. Thus, *PC* is used as the phase of coefficient with maximal local sharpness. Since image can be regarded as a 2-D signal [18], *PC* of image at location (x, y) can be calculated by Eq. 3.

$$PC(x,y) = \frac{\sum_k E_{\theta_k}(x,y)}{\varepsilon + \sum_n \sum_k A_{n,\theta_k}(x,y)} \tag{3}$$

where θ_k is the orientation angle at k [18], A_{n,θ_k} denotes the amplitude of the n-th Fourier component and angle θ_k, and ε is a positive constant to remove the DC components of image signals. In this fusion framework, parameter ε is set to 0.001 [18], [21]. $E_{\theta_k}(x,y)$ can be calculated by Eq. 4.

$$E_{\theta_k}(x,y) = \sqrt{F^2{}_{\theta_k}(x,y) + H^2{}_{\theta_k}(x,y)} \tag{4}$$

where $F_{\theta_k}(x,y)$ and $H_{\theta_k}(x,y)$ can be calculated by Eq. 5 and 6 respectively.

$$F_{\theta_k}(x,y) = \sum_n e_{n,\theta_k}(x,y) \tag{5}$$

$$H_{\theta_k}(x,y) = \sum_n o_{n,\theta_k}(x,y) \tag{6}$$

In Eq. 5 and 6, $e_{n,\theta_k}(x,y)$ and $o_{n,\theta_k}(x,y)$ are convolution results of input image at location (x, y), that can be evaluated by Eq. 7.

$$[e_{n,\theta_k}(x,y), o_{n,\theta_k}(x,y)] = [I(x,y) * M_n^e, I(x,y) * M_n^o] \tag{7}$$

where $I(x, y)$ is the pixel value of image at location (x, y). M_n^e and M_n^o are the even- and odd-symmetric filters of 2-D log-Gabor at scale n.

As a contrast invariant, *PC* does not reflect local contrast changes [21]. To compensate for the lack of *PC*, a measure of sharpness change (*SCM*) in Eq. 8 is developed.

$$SCM(x,y) = \sum_{(x_0,y_0)\in\Omega_0} (I(x,y) - I(x_0,y_0))^2 \tag{8}$$

where Ω_0 represents a local area with a size of 3×3 entered at (x, y). (x_0, y_0) represents a pixel point in the local area of Ω_0. Meanwhile, to calculate the (x, y) neighborhood contrast, the local *SCM* (*LSCM*) is introduced and expressed as Eq. 9.

$$LSCM\ (x, y) = \sum_{a=-M}^{M} \sum_{b=-N}^{N} SCM\ (x + a, y + b) \tag{9}$$

where $(2M + 1) \times (2N + 1)$ denotes the size of neighborhood.

As *LSCM* and *PC* cannot fully reflect the local luminance information, local energy (*LE*) is introduced [18], and can be calculated by Eq. 10.

$$LE\ (x, y) = \sum_{a=-M}^{M} \sum_{b=-N}^{N} (I\ (x + a, y + b))^2 \tag{10}$$

Design a new activity measure (*NAM*) that uses *PC*, *LSCM*, and *LE* complement to measure different aspects of image information.

$$NAM(x, y) = (PC(x, y))^{\alpha_1} \cdot (LSCM(x, y))^{\beta_1} \cdot (LE(x, y))^{\gamma_1} \tag{11}$$

where α_1, β_1, and γ_1 are parameters used to adjust *PC*, *LSCM*, and *LE* in *NAM*. In this paper, the parameter α_1, β_1, and γ_1 are set to 1, 2, and 2 respectively [18], [38].

When *NAM* is obtained, the fused highpass subband image can be calculated by the rule proposed in Eq. 12.

$$H_F(x, y) = \begin{cases} H_A\ (x, y) & if\ Lmap_A\ (x, y) = 1 \\ H_B\ (x, y) & otherwise \end{cases} \tag{12}$$

where $H_F(x, y)$, $H_A(x, y)$, and $H_B(x, y)$ are highpass subband images of fused image and source image I_A and I_B respectively. $Lmap_i\ (x, y)$ denotes a decision map for the fusion of highpass subband, and can be calculated by Eq. 13.

$$Lmap_i\ (x, y) = \begin{cases} 1 & if\ \lceil S_i\ (x, y) \rceil > \dfrac{\tilde{M} \times \tilde{N}}{2} \\ 0 & otherwise \end{cases} \tag{13}$$

In Eq. 13, Ω_1 represents a sliding window with a size of $\tilde{M} \times \tilde{N}$, and is centered at (x, y) and K is the number of source images.

B. FUSION RULE OF LOWPASS SUBBANDS

Lowpass subbands contain most energy of source images that has a significant impact on the fusion performance. Although NSCT filters most detailed information as highpass subbands, the limited decomposition level of NSCT cannot filter all the detailed information of source images as highpass subbands. To fully preserve the structured and detailed information of lowpass subbands, a measure, that considers both structured information preservation and detailed information extraction, is constructed for the fusion of lowpass subband components in NSCT domain [24].

In the proposed method, two activity level measures are implemented to measure the structured information, which is weighted local energy (WLE) and weighted sum of eight-neighborhood based modified Laplacian (WSEML) respectively.

WLE is defined as Eq.15.

$$WLE(x, y) = \sum_{m=-r}^{r} \sum_{n=-r}^{r} W \times (m + r + 1, n + r + 1) \times L(x + m, y + n)^2 \tag{15}$$

where $L(x, y)$ represents the lowpass subband of source image at location (x, y), $WLE(x, y)$ represents the *WLE* of image at location (x, y), W is a $(2r + 1) \times (2r + 1)$ matrix, elements in W are set to 2^{2r-d}, r is the radius of matrix W, and d of each element represents its four-neighborhood distance to the center of matrix W. For example, when r is set to 1, the normalized matrix W is shown by Eq. 16.

$$\frac{1}{16} \begin{bmatrix} 1 & 2 & 1 \\ 2 & 4 & 2 \\ 1 & 2 & 1 \end{bmatrix} \tag{16}$$

WLE is used as the structure measure to preserve the structured information.

WSEML is a measure of detail extraction, that can be defined as Eq. 17.

$$WSEML(x, y) = \sum_{m=-r}^{r} \sum_{n=-r}^{r} W(m + r + 1, n + r + 1) \times EML(x + m, y + n) \tag{17}$$

W is the weighted matrix that has the same definition as Eq. 15, and *EML* is defined as Eq. 19. *EML* can make the full use of neighboring information. Thus the detailed information can be better measured by *EML*.

When *EML* and *WSEML* are obtained, the fused lowpass subband image can be calculated by the rule proposed in Eq. 19, where $L_F(x, y)$, $L_A(x, y)$, and $L_B(x, y)$ are lowpass subband images of fused image and source image I_A and I_B respectively. $WLE^N{}_A$ and $WSEML^N{}_B$ are the normalized *WSEML* of I_A and I_B respectively.

$$\begin{aligned} &EML(x, y) \\ &= |2L(x, y) - L(x - 1, y) - L(x + 1, y)| \\ &\quad + |2L(x, y) - L(x - 1, y) - L(x + 1, y)| \\ &\quad + \frac{1}{\sqrt{2}} |2L(x, y) - L(x - 1, y - 1) - L(x + 1, y + 1)| \\ &\quad + \frac{1}{\sqrt{2}} |2L(x, y) - L(x - 1, y + 1) - L(x + 1, y - 1)| \end{aligned} \tag{18}$$

$$L_F(x, y) = \begin{cases} L_A(x, y) & if\ 0.5 \cdot WLE^N{}_A(x, y) + 0.5 \\ & \cdot WSEML^N{}_A(x, y) \geq 0.5 \cdot WLE^N{}_B(x, y) \\ & + 0.5 \cdot WSEML^N{}_B(x, y) \\ L_B(x, y) & otherwise. \end{cases} \tag{19}$$

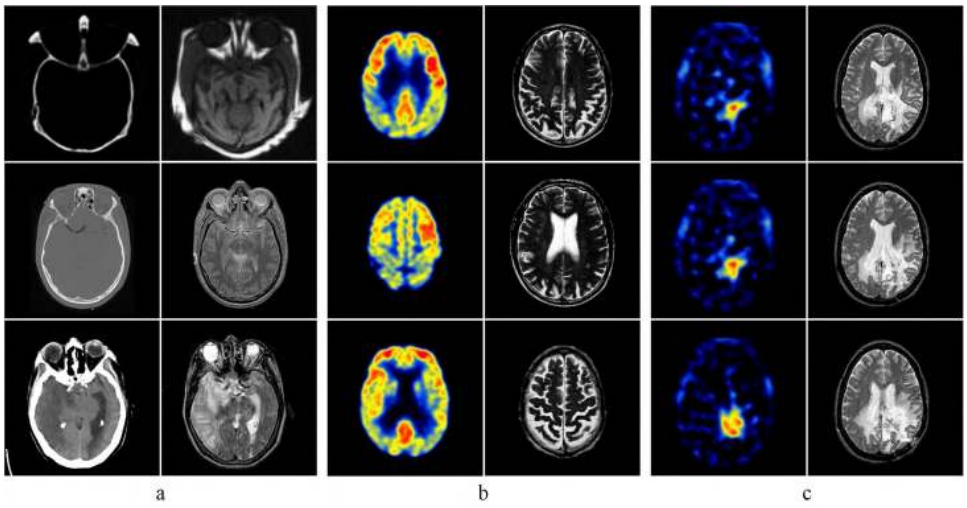

FIGURE 5. Source images of comparative experiments. (a), (b), and (c) are CT-MRI, MRI-PET, and SPECT-MRI source image pairs respectively.

When the fused coefficients of highpass subband H_F and lowpass subband L_F are calculated, the fused image I_F can be obtained by inverting NSCT [5], [7], [8] over $\{H_F, L_F\}$. The inverse transform of NSCT is realized by the optimal linear reconstruction [7] of highpass subband H_F and lowpass subband L_F using the dual coordinate system operator [7], [8].

IV. EXPERIMENTS AND ANALYSES

A. EXPERIMENT PREPARATION

In comparative experiments, nine pairs of computed tomography (CT) and magnetic resonance imaging (MRI) medical images, eight pairs of MRI and positron emission computed tomography (PET), and thirteen pairs of single-photon emission computed tomography (SPECT) and MRI medical images are used in the fusion performance testing respectively. The resolution of each test image is set to 256 × 256. Parts of representative images are shown in Fig. 5. In Fig. 5, image pairs (a), (b), and (c) show CT-MRI, MRI-PET, and SPECT-MRI image pairs respectively. Medical image pairs are obtained from *http://www.med.harvard.edu/aanlib/home.html*. All the experiments are programmed by Matlab 2014a and run on an Intel(R) Core(TM)i7-4790CPU @ 3.60GHz Desktop with 8.00 GB RAM.

Six mainstream medical image fusion methods published in recent four years, such as ASR [25], [36], KIM [13], MST [24], NSST [45], NSCT [10], and NSCT-PC [2] are compared with the proposed solution in comparative experiments. ASR is an adaptive sparse representation (ASR) model proposed by Liu *et al.* [25] for image fusion and denoising. KIM is a multi-modal image fusion method based on sparse representation proposed by Kim *et al.* [13]. MST is a general duty multi-modal image fusion algorithm based on MST and SR, proposed by Liu *et al.* [24]. NSST is a medical image fusion algorithm that combines PCNN and NSST proposed by Yin *et al.* [45]. Both NSCT and NSCT-PC are NSCT-based multi-modal medical image fusion algorithms, which are proposed by [10] and [2] respectively. NSCT-PC is a fusion framework that combines phase consistency and directive contrast in the NSCT domain. The fusions method selected in the comparative experiments contain three types of multi-modal image fusion framework: SR-based, NSCT-based, and MST- and SR-based fusion framework.

For quantitative evaluation, a single evaluation metric cannot fully reflect the quality of fused image. Therefore, several metrics are applied to making a comprehensive evaluation as necessary. In this paper, eight popular metrics are used to quantitatively evaluate the performance of different fusion methods, which are Q^{TE} [26], [32], Q^{IE} [26], [43], $Q^{AB/F}$ [33], [50], Q^{P} [26], [46], *MI* [37], Q^{Y} [26], [43], Q^{CB} [4], [26], and *VIF* [40].

Q^{TE} [26], [32] and Q^{IE} [26], [43] evaluate the Tsallis entropy and nonlinear correlation information entropy of fused images respectively. $Q^{AB/F}$ [33], [50] and Q^{P} [26], [46] are used to measure the edge information. $Q^{AB/F}$ [33] is a gradient-based quality index, and Q^{P} [26], [46] is an image fusion metric based on phase congruency. *MI* [26] and Q^{Y} [26], [43] measure the similarity between the fused image and source images. *MI* [26] as a quantitative measure

$$S_i(x,y) = \left\{ \begin{array}{l} (x_0,y_0) \in \Omega_1 | NAM_i(x_0,y_0) \geq \max(NAM_1(x_0,y_0), \\ \ldots, NAM_{i-1}(x_0,y_0), NAM_{i+1}(x_0,y_0), \ldots, NAM_K(x_0,y_0)) \end{array} \right\} \quad (14)$$

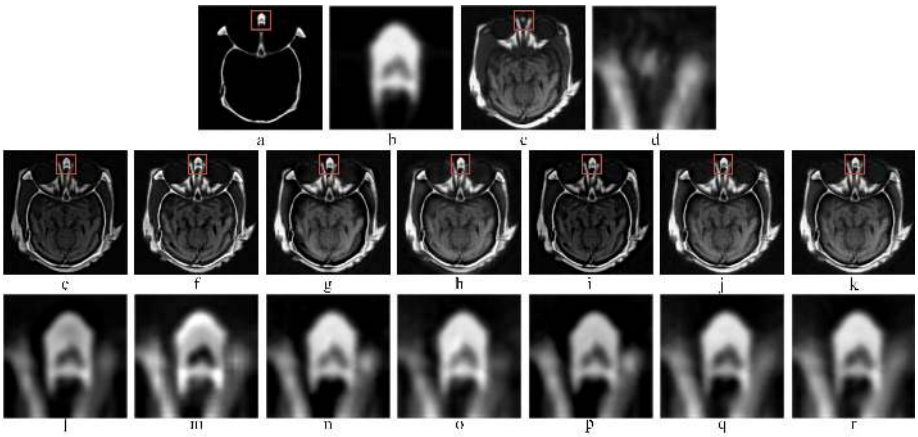

FIGURE 6. CT-MRI image fusion experiments, (a) and (c) are CT and MRI source images respectively. (b) and (d) are local detailed images of (a) and (c) respectively. (e), (f), (g), (h), (i), (j) and (k) are the fused images of ASR, JCPD, MST, NSST, NSCT, NSCT-PC and proposed methods respectively. (l), (m), (n), (o), (p), (q), and (r), are local detailed information of (e), (f), (g), (h), (i), (j) and (k) respectively.

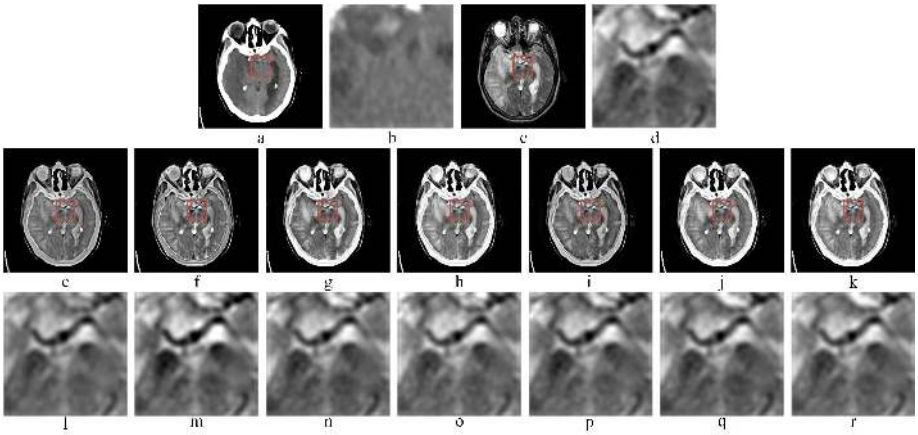

FIGURE 7. CT-MRI image fusion experiments, (a) and (c) are CT and MRI source images respectively. (b) and (d) are local detailed images of (a) and (c) respectively. (e), (f), (g), (h), (i), (j) and (k) are the fused images of ASR, JCPD, MST, NSST, NSCT, NSCT-PC and proposed methods respectively. (l), (m), (n), (o), (p), (q), and (r), are local detailed information of (e), (f), (g), (h), (i), (j) and (k) respectively.

evaluates the mutual dependence of two variables, and Q^Y [26], [43] is a structural similarity based metric for fusion assessment. Q^{CB} [4], [26] and *VIF* [40] evaluate the human visualization performance of fused images in different aspects. Q^{CB} [4], [26] is a fusion metric inspired by human perception. *VIF* [40] is the ratio between distorted testing image information and referenced image information.

For functional images such as PET and SPECT in medical images, it is feasible to use YUV color space to solve the fusion problem of grayscale and color images in the fusion process [23], [44]. The YUV space encodes the color image into one luminance component and two chrominance components, which fully takes into account human visual perception [23], [44], [45]. In the proposed fusion algorithm, the RGB color image is first converted into a YUV color space, and then three channel components of Y, U, and V are obtained. After that, the gray image and the Y channel component are applied to the fusion algorithm proposed in the third section to achieve image fusion. Finally, the fused Y-channel component, the source U-channel component, and the V-channel component are inversely transformed by YUV to obtain the fused color image.

B. EXPERIMENT RESULTS AND ANALYSES

1) COMPARISONS OF FUSION RESULTS

In cranial pathology, the fused image of CT-MRI images can provide both great visualization of bony anatomy and clear delineation of soft tissues. The typical CT-MRI fusion results of six popular image fusion methods are shown in Fig. 6 and 7. From (e), (f) and (g) of Fig. 6 and 7, it can easily figure out that the fused results of ASR, JCPD, MST, and NSCT lose a lot of energy in CT modality. The loss of energy causes the contrast decreasing of fused image. The contrast decreasing of fused image can seriously

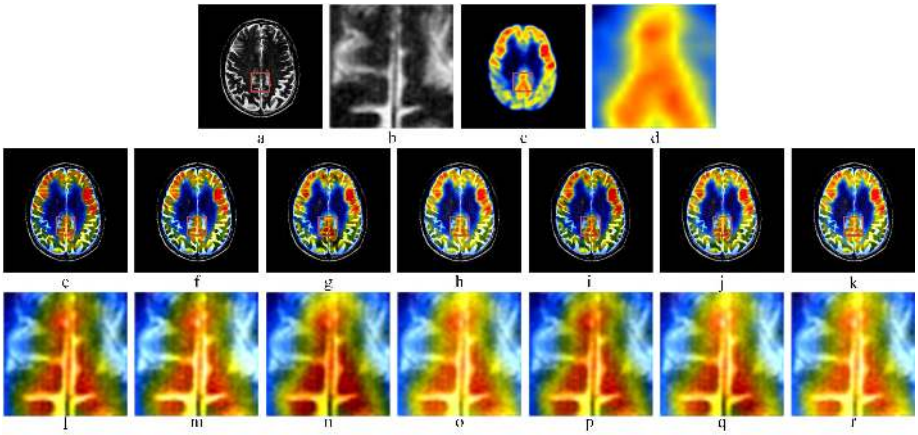

FIGURE 8. MRI-PET image fusion experiments, (a) and (c) are MRI and PET source images respectively. (b) and (d) are the local detailed images of (a) and (c) respectively. (e), (f), (g), (h), (i), (j) and (k) are the fused images of ASR, JCPD, MST, NSST, NSCT, NSCT-PC and proposed methods respectively. (l), (m), (n), (o), (p), (q), and (r), are local detailed information of (e), (f), (g), (h), (i), (j) and (k) respectively.

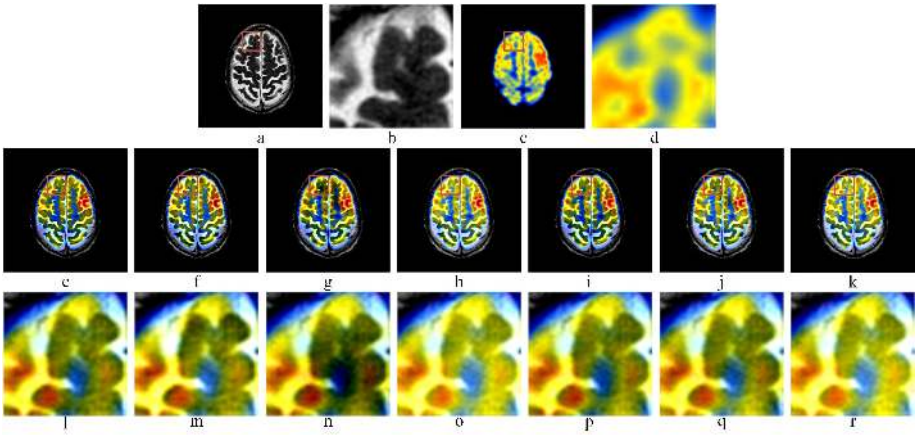

FIGURE 9. MRI-PET image fusion experiments, (a) and (c) are MRI and PET source images respectively. (b) and (d) are the local detailed images of (a) and (c) respectively. (e), (f), (g), (h), (i), (j) and (k) are the fused images of ASR, JCPD, MST, NSST, NSCT, NSCT-PC and proposed methods respectively. (l), (m), (n), (o), (p), (q), and (r), are local detailed information of (e), (f), (g), (h), (i), (j) and (k) respectively.

affect the accuracy of medical diagnosis, that is not acceptable in medical imaging fields. The intermediate regions of Fig.6 (e), (f), (g) and (i) show varying degrees of detail loss due to the decreasing of image contrast. The fused results of NSST, NSCT-PC and proposed method shown in Fig. 6 and 7 have great information preservation of both MRI and CT modality. However after furtherly exploring the detailed information shown in Fig. 7 (o), (q) and (r), it can find that NSST, and NSCT-PC lose parts of detailed information in CT modality, and the proposed method shows the great performance in preserving both CT and MRI modality information. Specifically, the structure and edge details of the right region of Fig.6 (o) and (q) are missing, while the overall structure and details of Fig.6 (r) are well preserved. The proposed method performs well on both the preservation of structured information and detailed information in fused CT-MRI image.

The fusion of MRI-PET image pair can provide clear soft tissues and metabolism of specific tissues, that are extensively used in medical diagnosis [12]. Fig. 8 and 9 show the fused results of four MRI-PET image pairs. The structured information of PET modality is missing in the fused results of ASR, JCPD, MST and NSCT shown in (e), (f), (g) and (i) of Fig. 8 and 9. The loss of PET modality can cause the medical misdiagnosis. Both the upper left brain in (e), (f), (g) and (i) of Fig. 8 and the center of brain in (e), (f), (g) and (i) of Fig. 9, the partial structure and edge details are lost. Especially in Fig. 9, the energy preservation results of ASR, MST, and NSCT fusion results are poor. All three methods NSST, NSCT-PC and the proposed method show great performance in multi-modality energy preservation. Comparing the detailed information of proposed method, NSST, and NSCT-PC shown in (r), (o) and (q) of Fig. 8 and 9, the proposed method has a little bit higher contrast than NSST,

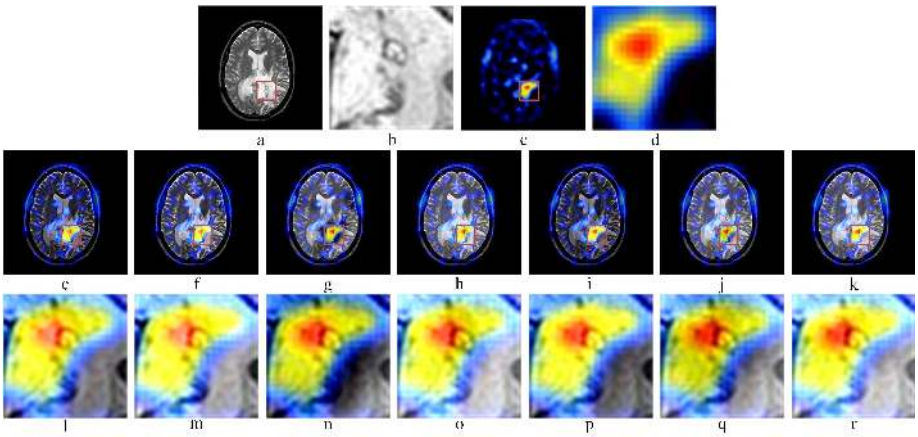

FIGURE 10. SPECT-MRI image fusion experiments, (a) and (c) are MRI and SPECT source images respectively. (b) and (d) are the local detailed images of (a) and (c) respectively. (e), (f), (g), (h), (i), (j) and (k) are the fused images of ASR, JCPD, MST, NSST, NSCT, NSCT-PC and proposed methods respectively. (l), (m), (n), (o), (p), (q), and (r), are local detailed information of (e), (f), (g), (h), (i), (j) and (k) respectively.

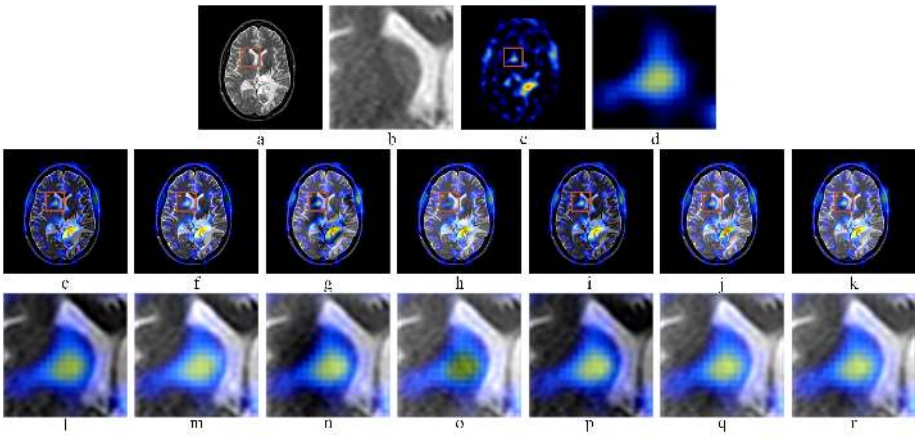

FIGURE 11. SPECT-MRI image fusion experiments, (a) and (c) are MRI and SPECT source images respectively. (b) and (d) are the local detailed images of (a) and (c) respectively. (e), (f), (g), (h), (i), (j) and (k) are the fused images of ASR, JCPD, MST, NSST, NSCT, NSCT-PC and proposed methods respectively. (l), (m), (n), (o), (p), (q), and (r), are local detailed information of (e), (f), (g), (h), (i), (j) and (k) respectively.

and has higher sharpness than NSCT-PC. For PET-MRI image fusion, the proposed method achieves excellent performance in both structured information preservation and detailed information extraction.

SPECT-MRI image fusion is often used to reflect the soft tissues and organism's metabolism [31]. The fused results of ASR, JCPD, MST, NSST, NSCT, NSCT-PC and proposed methods are demonstrated in Fig. 10 and 11. The performances of ASR, JCPD and NSCT on preserving the structured information of MRI modality are poor. MRI information is missing in the fused images of ASR, JCPD and NSCT. The gradation contrast of results fused by ASR and NSCT is poor, and some MRI texture and structure details are not sharpness. MST preserves most MRI and PET structured information well. However, a number of dark areas that appear in the fused image of MST affect the performance of fused image. NSST, NSCT-PC, and proposed method have excellent performance in the structured information preservation. However, a dark area appears at the edge of Fig.10 (q), which reduces the local image contrast. The soft tissue of Fig.10 (o) has a smoother edge and a brighter contrast, which may cause the loss of some important details. Comparing the detailed information shown in (o) and (r) of Fig. 10 and 11, the proposed method shows better contrast and sharpness than both NSST and NSCT-PC. So the proposed method achieves the best performance in both structured information preservation and detailed information extraction in SPECT-MRI image fusion.

2) OBJECTIVE EVALUATION ANALYSES

In this paper, eight objective metrics are applied to the evaluation of fusion performance. The average scores of ASR, JCPD, MST, NSST, NSCT, NSCT-PC, and proposed method for CT-MRI, MRI-PET, and SPECT-MRI

TABLE 1. Objective metrics of multi-modality medical image fusion experiment.

$CT-MRI$	Q^{TE}	Q^{IE}	$Q^{AB/F}$	Q^{P}	MI	Q^{Y}	Q^{CB}	VIF
ASR	0.4771	0.8060	0.4361	0.5304	1.7345	0.5051	0.3398	0.2901
JCPD	0.4791	0.8067	0.5680	0.4749	1.8412	0.6223	0.3444	0.3003
MST	0.5269	0.8084	0.8070	0.5120	2.0879	0.8442	0.3722	**0.3784**
NSST	0.4230	0.8060	0.7302	0.4879	1.7097	0.7766	0.3402	0.3160
NSCT	0.4159	0.8051	0.6369	0.5432	1.5441	0.6557	**0.3826**	0.3374
NSCT-PC	0.5120	0.8084	0.8383	0.5362	2.0824	0.8730	0.3538	0.3680
Proposed	**0.5460**	**0.8094**	**0.8502**	**0.5455**	**2.2188**	**0.8854**	0.3502	0.3745
$MRI-PET$	Q^{TE}	Q^{IE}	$Q^{AB/F}$	Q^{P}	MI	Q^{Y}	Q^{CB}	VIF
ASR	**0.8179**	0.8058	0.2907	**0.5659**	1.6756	0.3345	0.7598	0.3024
JCPD	0.8020	0.8057	0.2953	0.5530	1.6504	0.3397	**0.7634**	0.2925
MST	0.7307	0.8055	0.3108	0.4514	1.6451	0.3547	0.6919	0.2752
NSST	0.7612	**0.8059**	0.3231	0.5004	1.7155	0.3643	0.7036	0.3033
NSCT	0.7584	0.8057	0.3048	0.4795	1.6701	0.359	0.6518	0.2951
NSCT-PC	0.7464	**0.8059**	0.3208	0.5299	1.7064	0.3705	0.6809	0.302
Proposed	0.7659	**0.8059**	**0.3475**	0.5359	**1.7422**	**0.3731**	0.6708	**0.3191**
$SPECT-MRI$	Q^{TE}	Q^{IE}	$Q^{AB/F}$	Q^{P}	MI	Q^{Y}	Q^{CB}	VIF
ASR	0.6911	0.8059	0.3615	0.4969	1.8807	0.3643	0.5702	0.3144
JCPD	0.7419	0.8067	0.4061	0.5726	2.0610	0.4078	0.5741	0.3652
MST	0.7831	0.8084	0.5354	0.4991	2.3378	0.5266	**0.5947**	0.3901
NSST	0.8391	0.8097	0.5354	**0.6358**	2.5579	0.5508	0.5758	0.4406
NSCT	0.6714	0.8062	0.4554	0.5060	1.9408	0.4685	0.5685	0.3327
NSCT-PC	0.8095	0.8095	0.5236	0.5721	2.5202	0.5138	0.5544	0.4331
Proposed	**0.8675**	**0.8101**	**0.5455**	0.5997	**2.6134**	0.5187	0.5544	**0.4454**

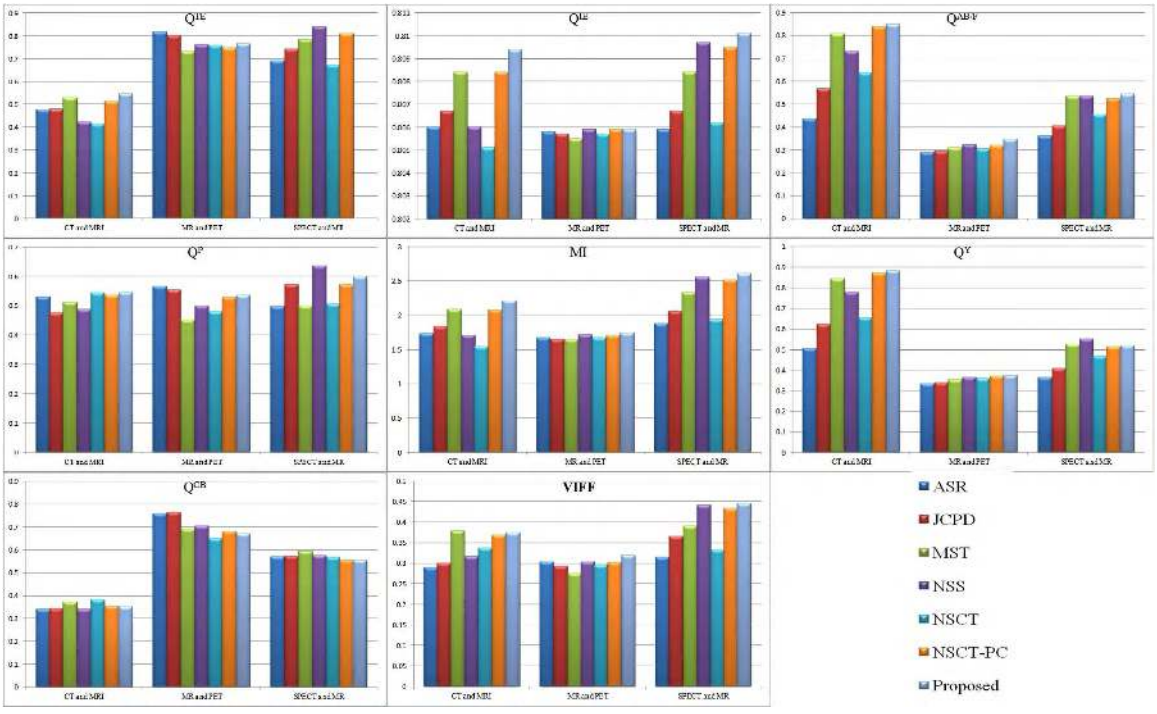

FIGURE 12. Objective evaluations of CT-MRI, MRI-PET, and SPECT-MRI mdical image fusion experiment.

image fusion are reported in Tab. 1. The highest value of each metrics is marked in bold. Tab. 1 is visualized in Fig. 12.

Comparing with other six methods, the proposed method gets the top rank in 6 of 8 objective metrics for CT-MRI image fusion. For MRI-PET and SPECT-MRI image fusion, the

TABLE 2. Computation cost comparison for both gray-level and color image fusion.

	$Gray-levelImageFusionTime$	$ColorImageFusionTime$
ASR	25.1237	25.7497
JCPD	19.2724	18.9828
MST	10.8807	9.6379
NSST	**1.9926**	**1.9754**
NSCT	3.7537	3.8051
NSCT-PC	31.6872	34.1270
Proposed	3.2948	3.9820

proposed method achieves the top in 5 of 8 objective metrics. Overall, the proposed method has the best performance in most cases of eight objective metrics among all three different types of multi-modality medical image fusion. In Fig. 12, the proposed method also obtains the top two scores in most comparisons.

The proposed method only ranks at the third place for Q^P of both SPECT-MRI and MRI-PET images fusion. NSST and ASR obtain higher score than the proposed method in SPECT-MRI and MRI-PET images fusion respectively. Q^P is used for phase congruency evaluation. The fused results of NSST lose the brightness information that the bright area in MRI image. The results fused by ASR have poor performance in the preservation of structured information in dark areas. Since the contrast of ASR and NSST relatively increases, the corresponding Q^P increases. In the objective score of human visual system, although the proposed method does not obtain the top three result in Q^{CB} of SPECT-MRI and MRI-PET images fusion, it still gets a good performance in *VIF*. According to the comparisons, the proposed method has a good robustness.

3) COMPUTATION COSTS ANALYSES

In comparative experiments, CT-MRI fusion uses gray-level image pairs. MRI-PET and SPECT-MRI image fusion use color image pairs. For each method, average computation costs of both gray-level and color image fusion are demonstrated in Tab. 2. Although the computation cost of proposed method is higher than NSST, it is still comparable. Although the complexity of the proposed method in color image fusion is higher than NSCT, the proposed method consumes significantly less time in grayscale image fusion than NSCT. In addition, the other methods are less efficient than the proposed method. The processing time of ASR and JCPD are 4 times greater than the proposed method. Meanwhile, the processing time of MST and NSCT-PC is 2 and 9 times greater than the proposed method respectively. The computation efficiency of proposed method can satisfy different usages in practice.

V. CONCLUSION AND DISCUSSION

In this paper, it proposes a phase congruency and local Laplacian energy based multi-modality medical image fusion method in NSCT domain. The presented method consists of three steps. First, it decomposes the source medical image pairs into highpass and lowpass subbands by NSCT. Then the highpass and lowpass subbands are fused by the proposed phase congruency and local Laplacian energy based fusion rule respectively. Finally, the integrated highpass and lowpass subbands are inversely transformed into the fused image. The experiment results demonstrate that the proposed method not only outperforms visual and objective quality in fused image, but also has competitive computation costs.

According to experiment results, the proposed method does not achieve great fusion performance in human visualization based objective metrics like PET-MRI image fusion. Additionally, although the proposed method obtains better fusion results than NSST, the computation costs of proposed method is higher than NSST. In future, the lowpass subbands fusion rule will be optimized to furtherly improve the performance of human visualization. It will also improve the computation efficiency for phase congruency based fusion rule.

REFERENCES

[1] A. Baghaie, S. Schnell, A. Bakhshinejad, M. F. Fathi, R. M. D'Souza, and V. L. Rayz, "Curvelet transform-based volume fusion for correcting signal loss artifacts in time-of-flight magnetic resonance angiography data," *Comput. Biol. Med.*, vol. 99, pp. 142–153, Jun. 2018.
[2] G. Bhatnagar, Q. M. J. Wu, and Z. Liu, "Directive contrast based multimodal medical image fusion in NSCT domain," *IEEE Trans. Multimedia*, vol. 9, no. 6, pp. 1014–1024, Aug. 2013.
[3] G. Bhatnagar, Q. M. J. Wu, and Z. Liu, "A new contrast based multimodal medical image fusion framework," *Neurocomputing*, vol. 157, pp. 143–152, Jun. 2015.
[4] Y. Chen and R. S. Blum, 'A new automated quality assessment algorithm for image fusion," *Image Vis. Comput.*, vol. 27, no. 10, pp. 1421–1432, 2009.
[5] A. L. da Cunha, J. Zhou, and M. N. Do, "The nonsubsampled contourlet transform: Theory, design, and applications," *IEEE Trans. Image Process.*, vol. 15, no. 10, pp. 3089–3101, Oct. 2006.
[6] S. Das and M. K. Kundu, "A neuro-fuzzy approach for medical image fusion," *IEEE Trans. Biomed. Eng.*, vol. 60, no. 12, pp. 3347–3353, Dec. 2013.
[7] M. N. Do and M. Vetterli, "Framing pyramids," *IEEE Trans. Signal Process.*, vol. 51, no. 9, pp. 2329–2342, Sep. 2003.
[8] M. N. Do and M. Vetterli, "The contourlet transform: An efficient directional multiresolution image representation," *IEEE Trans. Image Process.*, vol. 14, no. 12, pp. 2091–2106, Dec. 2005.
[9] J. Du, W. Li, and B. Xiao, "Anatomical-functional image fusion by information of interest in local laplacian filtering domain," *IEEE Trans. Image Process.*, vol. 26, no. 12, pp. 5855–5866, Dec. 2017.
[10] P. Ganasala and V. Kumar, "CT and MR image fusion scheme in nonsubsampled contourlet transform domain," *J. Digit. Imag.*, vol. 27, no. 3, pp. 407–418, 2014.

[11] J. Gong, B. Wang, L. Qiao, J. Xu, and Z. Zhang, "Image fusion method based on improved NSCT transform and PCNN model," in *Proc. Int. Symp. Comput. Intell. Design*, Dec. 2016, pp. 28–31.
[12] M. Haddadpour, S. Daneshavar, and H. Seyedarabi, "PET and MRI image fusion based on combination of 2-D Hilbert transform and IHS method," *Biomed. J.*, vol. 40, no. 4, pp. 219–225, 2017.
[13] M. Kim, D. K. Han, and H. Ko, "Joint patch clustering-based dictionary learning for multimodal image fusion," *Inf. Fusion*, vol. 27, pp. 198–214, Jan. 2016.
[14] H. Li, X. He, D. Tao, Y. Tang, and R. Wang, "Joint medical image fusion, denoising and enhancement via discriminative low-rank sparse dictionaries learning," *Pattern Recognit.*, vol. 79, pp. 130–146, Jul. 2018.
[15] H. Li, X. Li, Z. Yu, and C. Mao, "Multifocus image fusion by combining with mixed-order structure tensors and multiscale neighborhood," *Inf. Sci.*, vols. 349–350, pp. 25–49, Jul. 2016.
[16] H. Li, X. Liu, Z. Yu, and Y. Zhang, "Performance improvement scheme of multifocus image fusion derived by difference images," *Signal Process.*, vol. 128, pp. 474–493, Nov. 2016.
[17] H. Li, H. Qiu, Z. Yu, and B. Li, "Multifocus image fusion via fixed window technique of multiscale images and non-local means filtering," *Signal Process.*, vol. 138, pp. 71–85, Sep. 2017.
[18] H. Li, H. Qiu, Z. Yu, and Y. Zhang, "Infrared and visible image fusion scheme based on NSCT and low-level visual features," *Infr. Phys. Technol.*, vol. 76, pp. 174–184, May 2016.
[19] T. Li and Y. Wang, "Biological image fusion using a NSCT based variable-weight method," *Inf. Fusion*, vol. 12, no. 2, pp. 85–92, 2011.
[20] Y. Li, Y. Sun, X. Huang, G. Qi, M. Zheng, and Z. Zhu, "An image fusion method based on sparse representation and sum modified-Laplacian in NSCT domain," *Entropy*, vol. 20, no. 7, p. 522, 2018.
[21] Z. Lin, Z. Lei, X. Mou, and D. Zhang, "FSIM: A feature similarity index for image quality assessment," *IEEE Trans. Image Process.*, vol. 20, no. 8, pp. 2378–2386, Aug. 2011.
[22] X. Liu, Y. Zhou, and J. Wang, "Image fusion based on shearlet transform and regional features," *AEUE-Int. J. Electron. Commun.*, vol. 68, no. 6, pp. 471–477, 2014.
[23] Y. Liu, X. Chen, J. Cheng, and H. Peng, "A medical image fusion method based on convolutional neural networks," in *Proc. Int. Conf. Inf. Fusion*, 2017, pp. 1–7.
[24] Y. Liu, S. Liu, and Z. Wang, "A general framework for image fusion based on multi-scale transform and sparse representation," *Inf. Fusion*, vol. 24, pp. 147–164, Jul. 2015.
[25] Y. Liu and Z. Wang, "Simultaneous image fusion and denoising with adaptive sparse representation," *IET Image Process.*, vol. 9, no. 5, pp. 347–357, 2015.
[26] Z. Liu, E. Blasch, Z. Xue, J. Zhao, R. Laganiere, and W. Wu, "Objective assessment of multiresolution image fusion algorithms for context enhancement in night vision: A comparative study," *IEEE Trans. Pattern Anal. Mach. Intell.*, vol. 34, no. 1, pp. 94–109, Jan. 2012.
[27] K. Ma, Z. Duanmu, H. Yeganeh, and Z. Wang, "Multi-exposure image fusion by optimizing a structural similarity index," *IEEE Trans. Comput. Imag.*, vol. 4, no. 1, pp. 60–72, Mar. 2018.
[28] K. Ma, H. Li, H. Yong, Z. Wang, D. Meng, and L. Zhang, "Robust multi-exposure image fusion: A structural patch decomposition approach," *IEEE Trans. Image Process.*, vol. 26, no. 5, pp. 2519–2532, May 2017.
[29] M. Manchanda and R. Sharma, "An improved multimodal medical image fusion algorithm based on fuzzy transform," *J. Vis. Commun. Image Represent.*, vol. 51, pp. 76–94, Feb. 2018.
[30] F. Meskine, M. C. E. Mezouar, and N. Taleb, "A Rigid image registration based on the nonsubsampled contourlet transform and genetic algorithms," *Sensors*, vol. 10, no. 9, pp. 8553–8571, 2010.
[31] R. Misri, D. Meier, A. C. Yung, P. Kozlowski, and U. O. Häfeli, "Development and evaluation of a dual-modality (MRI/SPECT) molecular imaging bioprobe," *Nanomed. Nanotechnol. Biol. Med.*, vol. 8, no. 6, pp. 1007–1016, 2012.
[32] R. Nava, B. Escalante-Ramirez, and G. Cristóbal, "Mutual information improves image fusion quality assessments," *SPIE News Room*, 2007.
[33] V. Petrović, "Subjective tests for image fusion evaluation and objective metric validation," *Inf. Fusion*, vol. 8, no. 2, pp. 208–216, 2007.
[34] G. Qi, J. Wang, Q. Zhang, F. Zeng, and Z. Zhu, "An integrated dictionary-learning entropy-based medical image fusion framework," *Future Internet*, vol. 9, no. 4, p. 61, 2017.
[35] G. Qi, Q. Zhang, F. Zeng, J. Wang, and Z. Zhu, "Multi-focus image fusion via morphological similarity-based dictionary construction and sparse representation," *CAAI Trans. Intell. Technol.*, vol. 3, no. 11, pp. 83–94, Jun. 2018.
[36] G. Qi, Z. Zhu, K. Erqinhu, Y. Chen, Y. Chai, and J. Sun, "Fault-diagnosis for reciprocating compressors using big data and machine learning," *Simul. Model. Pract. Theory*, vol. 80, pp. 104–127, Jan. 2018.
[37] G. Qu, D. Zhang, and P. Yan, "Information measure for performance of image fusion," *Electron. Lett.*, vol. 38, no. 7, pp. 313–315, Mar. 2002.
[38] X.-B. Qu, J.-W. Yan, H.-Z. Xiao, and Z.-Q. Zhu, "Image fusion algorithm based on spatial frequency-motivated pulse coupled neural networks in nonsubsampled contourlet transform domain," *Acta Autom. Sin.*, vol. 34, no. 12, pp. 1508–1514, 2008.
[39] F. Shabanzade and H. Ghassemian, "Multimodal image fusion via sparse representation and clustering-based dictionary learning algorithm in nonsubsampled contourlet domain," in *Proc. Int. Symp. Telecommun.*, Sep. 2017, pp. 472–477.
[40] H. R. Sheikh and A. C. Bovik, *Image Information and Visual Quality*. Piscataway, NJ, USA: IEEE Press, 2006.
[41] K. Wang, G. Qi, Z. Zhu, and Y. Chai, "A novel geometric dictionary construction approach for sparse representation based image fusion," *Entropy*, vol. 19, no. 7, p. 306, 2017.
[42] J. Xia, Y. Chen, A. Chen, and Y. Chen, "Medical image fusion based on sparse representation and PCNN in NSCT domain," *Comput. Math. Methods Med.*, vol. 2018, no. 5, pp. 1–12, 2018.
[43] C. Yang, J.-Q. Zhang, X.-R. Wang, and X. Liu, "A novel similarity based quality metric for image fusion," *Inf. Fusion*, vol. 9, no. 2, pp. 156–160, 2008.
[44] Y. Yang, Y. Que, S. Huang, and P. Lin, "Multimodal sensor medical image fusion based on type-2 fuzzy logic in NSCT domain," *IEEE Sensors J.*, vol. 16, no. 10, pp. 3735–3745, May 2016.
[45] M. Yin, X. Liu, Y. Liu, and X. Chen, "Medical image fusion with parameter-adaptive pulse coupled neural network in nonsubsampled shearlet transform domain," *IEEE Trans. Instrum. Meas.*, vol. 68, no. 1, pp. 49–64, Jan. 2018.
[46] J. Zhao, R. Laganiere, and Z. Liu, "Performance assessment of combinative pixel-level image fusion based on an absolute feature measurement," *Int. J. Innov. Comput. Inf. Control*, vol. 3, no. 6, pp. 1433–1447, 2007.
[47] Z. Zhu, Y. Chai, H. Yin, Y. Li, and Z. Liu, "A novel dictionary learning approach for multi-modality medical image fusion," *Neurocomputing*, vol. 214, pp. 471–482, Nov. 2016.
[48] Z. Zhu, G. Qi, Y. Chai, and Y. Chen, "A novel multi-focus image fusion method based on stochastic coordinate coding and local density peaks clustering," *Future Internet*, vol. 8, no. 4, p. 53, 2016.
[49] Z. Zhu, G. Qi, Y. Chai, and P. Li, "A geometric dictionary learning based approach for fluorescence spectroscopy image fusion," *Appl. Sci.*, vol. 7, no. 2, p. 161, 2017.
[50] Z. Zhu, G. Qi, Y. Chai, H. Yin, and J. Sun, "A novel visible-infrared image fusion framework for smart city," *Int. J. Simul. Process Model.*, vol. 13, no. 2, pp. 144–155, May 2018.
[51] Z. Zhu, J. Sun, G. Qi, Y. Chai, and Y. Chen, "Frequency regulation of power systems with self-triggered control under the consideration of communication costs," *Appl. Sci.*, vol. 7, no. 7, p. 688, 2017.
[52] Z. Zhu, H. Yin, Y. Chai, Y. Li, and G. Qi, "A novel multi-modality image fusion method based on image decomposition and sparse representation," *Inf. Sci.*, vol. 432, pp. 516–529, Mar. 2018.

ZHIQIN ZHU received the B.E. and Ph.D. degrees from Chongqing University, in 2010 and 2016, respectively. He is currently a Lecturer with the Automation College, Chongqing University of Post and Telecommunications. He has presided over funds of the National Science Foundation of China and the Educational Department of Chongqing. His primary research interests include machine learning and image processing.

MINGYAO ZHENG was born in 1995. She is currently pursuing the master's degree in control engineering with the Automation College, Chongqing University of Post and Telecommunications. Her main research interest includes image processing.

GUANQIU QI received the Ph.D. degree in computer science from Arizona State University, in 2014. He is currently an Assistant Professor with the Department of Mathematics and Computer and Information Science, Mansfield University of Pennsylvania, USA. His primary research interests include many aspects of software engineering, such as software-as-a-service, testing-as-a-service, big data testing, combinatorial testing, and service-oriented computing, and machine learning and image processing.

DI WANG received the B.Sc. degree in electronic information engineering and the M.Sc. degree in software engineering from Chongqing University, China, in 2010 and 2014, respectively, where she is currently pursuing the Ph.D. degree. After her B.Sc. degree, she was an Electronic Engineer in one Taiwanese capital corporate in Shanghai for more than one year. Her current research interests include systems modeling, intelligent systems, sensors, and information processing.

YAN XIANG received the B.E. degree in engineering and the M.S. degree in science from Wuhan University. She is currently a Lecturer with the Kunming University of Science and Technology. She has presided over a fund of the Yunnan Provincial Education Department, a Youth Fund of the Kunming University of Technology, and the Key Computer Laboratory Project of Yunnan province. Her main research interests include image processing, text mining, and machine learning.